JOURNAL OF AGRICULTURAL AND FOOD CHEMISTRY

pubs.acs.org/JAFC Article

Engineering the Thermostability of a D-Carbamoylase Based on Ancestral Sequence Reconstruction for the Efficient Synthesis of D-Tryptophan

Jiamin Hu, Xiaoyu Chen, Lu Zhang, Jieyu Zhou, Guochao Xu,* and Ye Ni*

Cite This: J. Agric. Food Chem. 2023, 71, 660−670 Read Online

ACCESS | Metrics & More | Article Recommendations | Supporting Information

ABSTRACT: Employing ancestral sequence reconstruction and consensus sequence analysis, the thermostability of a novel D-carbamoylase derived from *Nitratireductor indicus* (*Ni*HyuC) was engineered through greedy-oriented iterative combinatorial mutagenesis. A mutant S202P/E208D/R277L (M4Th3) was obtained with significantly elevated thermostability. M4Th3 has a half-life of 36.5 h at 40 °C, about 28.5 times of 1.3 h of its parent M4. For the reaction at 40 °C, M4Th3 can catalyze 10 mM *N*-carbamoyl-D-tryptophan to produce D-tryptophan with a conversion ratio of 96.4% after 12 h, which is significantly higher than 64.1% of M4. MD simulation reveals that new hydrogen bonds emerging from E208D on the surface can increase the hydrophobicity of the protein, leading to improved stability. More importantly, R277L could contribute to enhanced interface stability of homodimeric M4. This study provides a thermostable D-carbamoylase for the "hydantoinase process", which has potential in the industrial synthesis of optically pure natural and non-natural amino acids.

KEYWORDS: *D-carbamoylase, D-tryptophan, thermostability, ancestral sequence reconstruction, hydantoinase process*

1. INTRODUCTION

D-Amino acids are important non-natural amino acids and are widely used in food, agriculture, cosmetics, and pharmaceuticals. For instance, alitame, an L-Asp-D-Ala dipeptide sweetener, is about 10 times sweeter than aspartame (L-Asp-L-(αMe)Phe) and 2000 times sweeter than sucrose.[1] D-Valine is useful in the preparation of pyrethroid insecticides.[2] D-Aspartic acid is used for the synthesis of aspirin[3] and is often added to cosmetics due to its antioxidative activity.[1] D-Tryptophan displays analgesic activity and can be used to prepare antibiotics, which are vital synthons for the synthesis of Tadalafil (cialis) and other related peptides[4−6] as well as Thymodepressin (γ-D-Glu-D-Trp).[7] In addition, D-tryptophan is considered as an effective food preservative and a promising substitute in the dairy industry.[8] Considering their wide application and increasing demand, the development of efficient methods for the synthesis of D-amino acids has become a prospective field in the amino acid industry.

Various approaches, including chemical and enzymatic methods, have been developed for the synthesis of D-tryptophan. Chemical methods are easily reproducible at a large scale; however, they are usually impeded by problems such as complicated reaction conditions, environmental pollution, and low stereoselectivity. Enzymatic approaches are advantageous in terms of green catalysts, fewer side reactions, high stereoselectivity, and mild reaction conditions. However, the activity and thermostability of enzymes are insufficient for industrial application.[9−11] The "hydantoinase process", comprising hydantoin racemase (HyuA), D/L-hydantoinase (HyuH), and D/L-carbamoylase (HyuC), is an important approach that has been widely applied in the preparation of optically active non-natural amino acids due to its high economy and high efficiency.[12−14] The "hydantoinase process" is of special interest in the synthesis of D-amino acids from the corresponding hydantoin with 100% theoretical yield.[12] Carbamoylase is generally regarded as the rate-limiting enzyme in the "hydantoinase process" due to its low efficiency and limited thermostability.[4,15] Previously, a novel D-carbamoylase derived from *Nitratireductor indicus* (*Ni*HyuC) was identified, engineered, and applied to the synthesis of D-tryptophan. Although the efficiency of *Ni*HyuC was increased by 44.2-fold, the inherent problem of poor thermostability still exists, with a half-life of merely 1.3 h at 40 °C.[4,15] Moreover, the solubility of hydantoin derivatives is usually low. Higher reaction temperatures could not only enhance the solubility of hydantoins but also promote the racemization of 5-monosubstituted hydantoins. As a result, the development of thermostable D-carbamoylase has drawn increasing attention.[4,16]

Enormous endeavors have been devoted to engineering enzymes with improved stability.[17−22] However, a generally applicable strategy for engineering the thermostability of various enzymes has yet to be established.[23] At present, several tools based on computational calculations and force field analysis have been developed, such as FoldX and Rosetta, which are time- and computation-intensive and rely on

Received: November 7, 2022
Revised: December 10, 2022
Accepted: December 12, 2022
Published: December 21, 2022

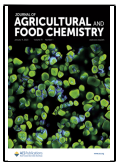

https://doi.org/10.1021/acs.jafc.2c07781
J. Agric. Food Chem. 2023, 71, 660−670

accurate protein structures and virtual saturation mutagenesis.[24−29] Moreover, when the structural and functional information of the protein is not fully understood, it is difficult to construct a rational design, let alone to predict the epistatic effect of combinatorial mutants.[30,31] It can be noted that most of the reported experimental and computational methods depend on site-directed saturation mutagenesis or screening of millions of candidates, which are labor- and computation-intensive. Ancestral sequence reconstruction (ASR) refers to the technique of deriving the amino acid sequences of ancestral enzymes of extinct organisms by computer algorithms. Reconstruction of ancestral sequences shows that enzymes from the Precambrian period are generally more thermostable than existing enzymes.[23,32] The most distinct advantage of ASR is the independence of a reliable protein structure.[33] Therefore, ASR technology has been developed to construct ancestral enzymes with improved thermostability or high catalytic promiscuity.[34−39] For example, an ancestor P450 enzyme identified using ASR technology can withstand temperatures 30 °C higher than those by the existing ones.[23]

In this study, we sought to employ ASR-guided evolutionary conservative analysis to engineer the thermostability of D-carbamoylase (*Ni*HyuC). To overcome the "trade-off" between activity and stability, greedy-oriented iterative mutagenesis was adopted. The application potential of a thermostable mutant was also evaluated in the synthesis of D-tryptophan. Mechanisms for enhanced thermostability were elucidated through deconvolution analysis and MD simulations. This study provides a thermostable D-carbamoylase for the "hydantoinase process", a well-known multienzyme cascade for producing chiral amino acids.

2. MATERIALS AND METHODS

2.1. Reagents and Strains. The substrate *N*-carbamoyl-D-tryptophan was synthesized according to the reported method.[40] Gene coding for mutant M4 of *Ni*HyuC was constructed in a previous study and used as the parent in this study.[4,15] Strain *Escherichia coli* BL21(DE3) was stored in the laboratory and used for gene expression.

2.2. Ancestral Sequence Reconstruction and Construction of Mutants. The ancestral sequence of *Ni*HyuC M4 was reconstructed through the FireProt-ASR online service website (http://loschmidt.chemi.muni.cz/fireprotasr/),[41] and the protein crystal structure of *Ni*HyuC M4 (PDB ID: 6LE2) was rationally analyzed according to the alignment results. Mutants with residual activity greater than M4 in the preliminary screening were selected for secondary screening to determine the half-life at 40 °C (i.e. $t_{1/2}$ (40 °C)). The half-life ($t_{1/2}$) refers to the time required to lose half of the enzyme activity at a given temperature.

2.3. Activity Assay. *2.3.1. Activity Assay.* The activity of D-carbamoylase was determined with *N*-carbamoyl-D-tryptophan as the substrate. Specifically, 10 μL of 1 mg·mL^{-1} enzyme solution (in 100 mM, pH 8.0, Tris-HCl) was added to 1 mL of the reaction system containing 2 mM *N*-carbamoyl-D-tryptophan (Table S3). After that, the reaction was conducted at 30 °C for 10 min and terminated with a threefold volume of methanol to determine the initial reaction rate.

2.3.2. Definition of Enzyme Activity. The amount of enzyme required to catalyze the conversion of *N*-carbamoyl-D-tryptophan to 1 μmol of D-tryptophan per min at 30 °C is defined as one unit (U).

2.3.3. Preliminary Screening. The residual activity of crude enzyme supernatants was measured after incubating at 40 °C for 15 min. The activity of the crude enzyme measured after incubating at 30 °C for 15 min was regarded as the control. Mutants with higher ratios of residual activities to the control compared with M4 were selected for secondary screening.

2.3.4. Secondary Screening. The mutants with residual activity greater than M4 (about 82%) in the preliminary screening were purified by Ni-NTA affinity chromatography. Then, the purified enzymes were diluted to 1 mg·mL^{-1} and incubated at 40 °C to test the $t_{1/2}$ values. Samples were withdrawn and subjected to the determination of residual activities. Initial incubation at 40 °C for 5 min was regarded as 100%. All assays were performed at least three times.

$$\text{relative activity}(\%) = \frac{\text{specific activity of mutant}}{\text{specific activity of M4}} \times 100\% \quad (1)$$

$$\text{residual activity}(\%) = \frac{\text{activity after incubation}}{\text{initial activity at 0 h}} \times 100\% \quad (2)$$

2.4. HPLC Analysis of the Substrate and Product. *N*-Carbamoyl-D-tryptophan and the product D-tryptophan were analyzed using an Agilent 1260 high-performance liquid chromatography (HPLC) system equipped with a ZORBAX SB-C_{18} column (25 cm × 4.6 mm, 5 μm), using 25% acetonitrile and 75% KH_2PO_4 (20 mM pH 2.5) (v/v) as the mobile phase at 30 °C, 210 nm. The flow rate was 1 mL·min^{-1}.

2.5. Characterization of Enzymatic Properties. *2.5.1. Optimal Temperature, T_{opt}.* The effect of temperature was evaluated by determining the initial reaction rates of M4 and mutants at 25−55 °C. The temperature at which enzymes display the highest activity is regarded as the optimum temperature, T_{opt}.

2.5.2. Half-Deactivation Temperature, T_{50}^{15}. The purified enzyme was diluted to 1 mg·mL^{-1} and incubated at different temperature gradients (35−55 °C) for 15 min. Then, the activity was measured following methods described in Section 2.3. The temperature at which the relative enzyme activity is lost by half is the T_{50}^{15}.

2.5.3. Activation Energy for Deactivation, E. The activation energy for the deactivation of the enzyme was calculated according to the Arrhenius equation after measuring the $t_{1/2}$ values at three different temperatures (40, 43, and 50 °C) using purified enzymes. The slope was obtained by plotting ln *k* against T^{-1}, and the activation energy for deactivation was then calculated.

$$\ln k = \ln A - \frac{E}{RT} \quad (3)$$

k: deactivation rate constant at different temperatures;
T: thermodynamic temperature, K;
R: molar gas constant, kJ·mol^{-1}·K^{-1};
E: activation energy for deactivation, kJ·mol^{-1};
A: pre-exponential factor, also known as the Arrhenius constant, has the same unit as *k*.

The purified enzymes were diluted to 1 mg·mL^{-1}. Then, 1 mL of the enzyme solution was withdrawn and incubated in a water bath at 40, 43, and 50 °C, and the activities were measured after different incubation times. All assays were performed in triplicates.

2.5.4. Melting Temperature, T_m. The purified enzymes were diluted to 1 mg·mL^{-1}. Using nano-differential scanning calorimetry (nano-DSC), the change in the heat capacity of the enzyme was determined at a scanning rate of 1 °C·min^{-1}. With an increase in the temperature from 20 to 80 °C, the protein is denatured and unfolded. Changes in the heat capacity were determined using NanoAnalyze (chose the TwoStateScaled model) to calculate its relatively accurate T_m values.

2.6. MD Simulations and B-Factor Analysis. Based on the crystal structure of M4, homology modeling of the mutant M4Th3 was performed by Discovery Studio 2021. Multiple molecular dynamics (MD) simulations (3 × 100 ns) of M4 and M4Th3 were performed using Gromacs 5.1.4. Based on the OPLS-AA/L all-atom force field, the cubic box was used as the unit cell, the SPC/E water model was selected, the system was equilibrated by adding the necessary ions to neutralize the net charge of the protein, and the MDRUN module was used for energy minimization. Then, NVT and NPT equilibration was performed after the system temperature was set to 303 K (or 313 K). During the MD process, the root-mean-

https://doi.org/10.1021/acs.jafc.2c07781
J. Agric. Food Chem. 2023, 71, 660−670

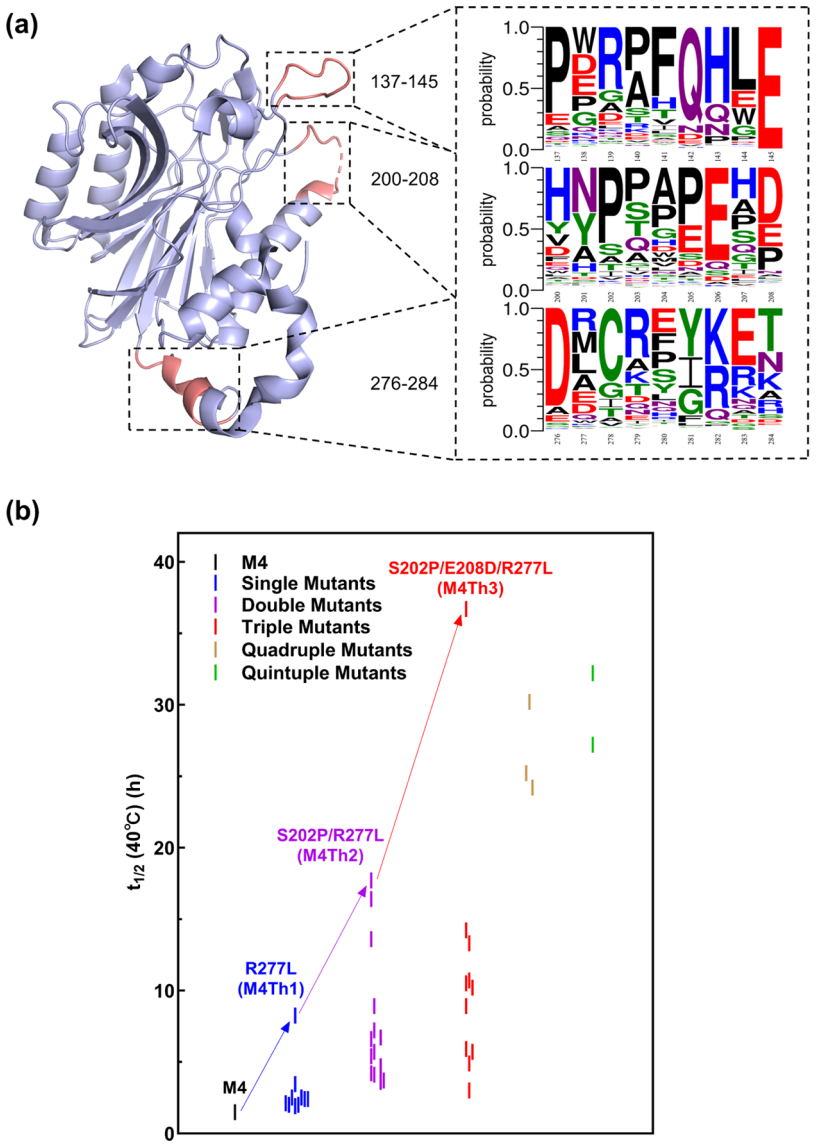

Figure 1. (a) Evolutionary conservation analysis of sites 137−145, 200−208, and 276−284 of all of the 299 D-carbamoylases reconstructed based on ancestral sequences. (b) Evolutionary routes of the thermostability of *Ni*HyuC. Black, M4; blue, single mutants; purple, double mutants; red, triple mutants; brown, quadruple mutants; green, quintuple mutants.

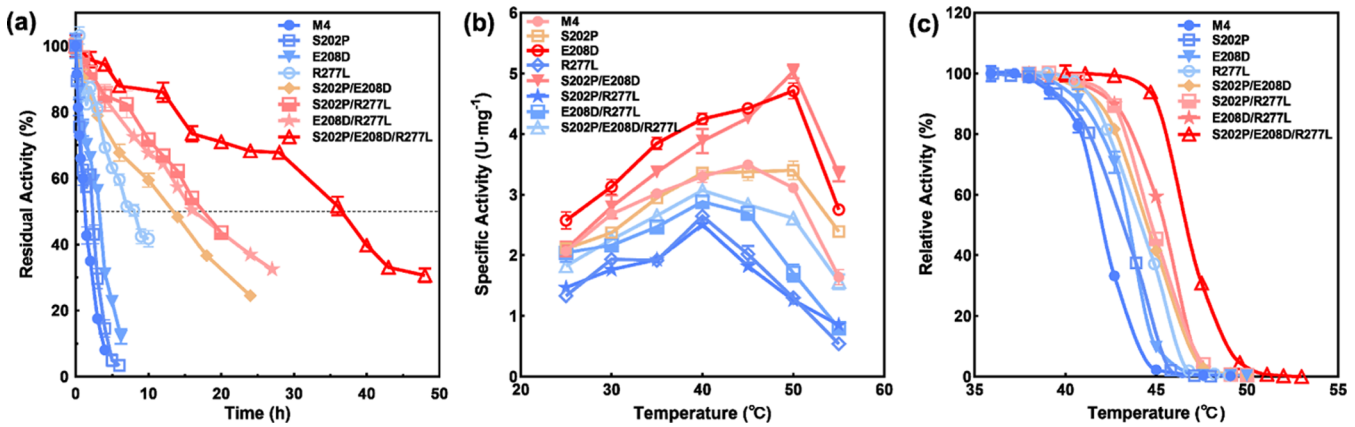

Figure 2. Thermostability at 40 °C (a), temperature−activity profiles (b), and kinetic stability (c) of S202P/E208D/R277L (M4Th3) and the corresponding single and double mutants.

square deviation (RMSD) of the conformation was calculated to measure the stability of the system; the root-mean-square fluctuation (RMSF) of each amino acid residue was retrieved. The radius of gyration (Rg) is not only an important indicator of the flexibility of

https://doi.org/10.1021/acs.jafc.2c07781
J. Agric. Food Chem. 2023, 71, 660−670

protein regions but also a parameter reflecting the tightness of the protein as well as its volume and shape. The larger the Rg, the more unstable the system.

The B-factors of M4 and M4Th3 were determined through the Hotspot Wizard online service website (http://loschmidt.chemi.muni.cz/hotspotwizard).[42]

2.7. Biotransformation Reaction for the Synthesis of D-Tryptophan. To further investigate and verify the feasibility of M4Th3 for the synthesis of D-tryptophan, reactions were performed to explore the reaction progress curves of M4Th3, M4, and WT at 30 and 40 °C (added according to Table S4), and the reactions were conducted for 12 h. At different time intervals, samples were withdrawn from the reaction system and mixed with a ninefold volume of methanol to terminate the reaction. The conversion ratios were determined using the HPLC method as above mentioned.

3. RESULTS AND DISCUSSION

3.1. Identification of Hotspots Based on Ancestral Sequence Reconstruction Analysis.

3.1.1. Reconstruction of Ancestral Sequences. A total of 149 predicted ancestral nodes and 150 descendant protein sequences in the database (299 in total) were obtained by ancestral sequence reconstruction (ASR). Three ancestral enzymes (Figure S1) from node 151 (located at the root), node 180 (at the intermediate node), and node 292 (adjacent to M4) were synthesized and inserted into vector pET-28a(+). After heterologous expression in *E. coli*, all three ancestral enzymes were expressed in the soluble form according to SDS-PAGE analysis (Figure S2). However, after reaction for 2 h, almost no D-tryptophan was detected. The undetectable activity is understandable, considering that the structure of the ancestral enzyme is distinct from its descendent counterpart. Generally, ancestral enzymes are expected to display higher thermostability. Therefore, the melting temperature (T_m) values of M4, node 151, node 180, and node 292 were measured. The T_m values of nodes 180 and 292 were 50.5 and 52.4 °C, respectively, higher than 46.8 °C of M4. However, the T_m value of node 151 was not measurable, likely due to its low protein concentration caused by the low binding affinity toward the Nickel column.

Furthermore, sequence alignments were conducted between M4 and node 151, node 180, and node 292 to analyze the possible evolutionary regions of M4 over time. That is, the regions that affect the thermostability of M4 could be inferred from ancestral sequences. Through comparison, it was found that the conservation of sites 137−145, 200−208, and 276−284 was low (Figure S3). Considering that the three selected ancestor nodes may not be representative, multiple sequence alignment was performed among the three amino acid sequences on M4 and 299 ancestor sequences obtained by ASR, and the evolutionary conservatism of amino acid residues was analyzed (Figure 1a).

Table 1. Kinetic Parameters of M4 and M4Th3

mutants	V_{max} (U·mg^{-1})	K_m (mM)	k_{cat}(min^{-1})	k_{cat}/K_m (min^{-1}·mM^{-1})
M4	3.40 ± 0.34	0.41 ± 0.02	118 ± 12	288
M4Th3	2.97 ± 0.39	0.34 ± 0.02	103 ± 14	302

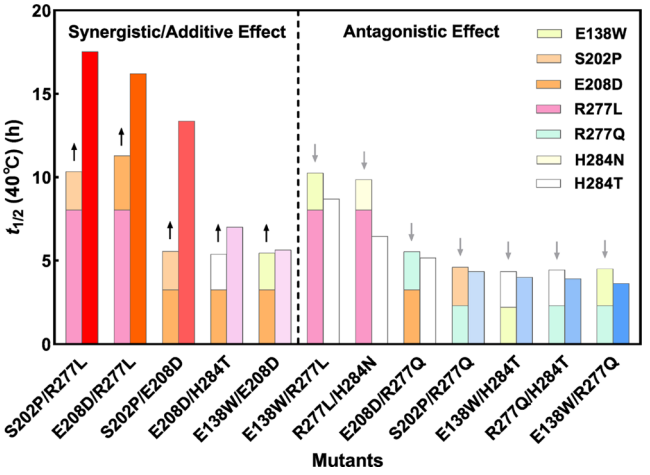

Figure 3. Cooperative interaction analysis of single and double mutants. The left side of each combination is the superposition of the $t_{1/2}$ (40 °C) of the two single points that constitute the double mutant, and the right side refers to the actual measured $t_{1/2}$ (40 °C) of the double mutant. The mutants are sorted from high to low by their $t_{1/2}$ values. Black upward arrow: two sites have a synergistic/additive effect; gray downward arrow: two sites have an antagonistic effect.

3.1.2. Identifying Hot Spots from Evolutionary Conservatism. In the crystal structure of M4 (PDB ID: 6LE2), residues 204 and 205 were absent in the loop 200−207, which was mainly attributed to their high flexibility. It is assumed that the thermostability can be improved by increasing rigidity and reducing flexibility. According to the results of the comparison of M4 with the 299 ancestor sequences, it was found that except for E206, sites N200, D201, S202, L203, S204, G205, and A207 are not conservative. Interestingly, the two highly conserved amino acids Asp and Glu at E208 on the α-helix are both acidic amino acids. As residues 200−208 are located at the entrance of the active pocket, smaller side chains would facilitate the access of the substrate into the active center and improve the enzyme activity. In previous studies, mutagenesis of N200 and A207 had been attempted to improve the catalytic efficiency, in which 3.4−4.4-fold improvement was achieved compared with *Ni*HyuC-WT.[4] As a result, sites D201,

Table 2. Characterization of the Properties of Thermostable Mutants

mutant	specific activity (U·mg^{-1})	T_{opt} (°C)	T_{50}^{15} (°C)	T_m (°C)	$t_{1/2}$(40 °C) (h)	$t_{1/2}$(43 °C) (h)	$t_{1/2}$(50 °C) (min)	E (kJ·mol^{-1})
M4	2.68 ± 0.01	45.0	42.0	46.8	1.3	0.1	0.4	435.7
S202P	2.37 ± 0.09	50.0	43.1	47.9	2.3	0.3	0.5	464.3
E208D	3.13 ± 0.22	50.0	43.5	48.1	3.3	0.5	0.5	504.1
R277L (M4Th1)	1.93 ± 0.13	40.0	44.2	48.1	8.0	0.9	0.7	546.9
S202P/E208D	2.80 ± 0.33	50.0	44.5	49.6	13.4	1.4	1.1	550.9
S202P/R277L (M4Th2)	1.76 ± 0.15	40.0	44.8	48.9	17.5	1.4	0.9	592.4
E208D/R277L	2.16 ± 0.06	40.0	45.4	49.2	16.2	2.5	0.9	589.4
S202P/E208D/R277L (M4Th3)	2.26 ± 0.22	40.0	46.7	50.3	36.5	4.0	1.2	636.1

https://doi.org/10.1021/acs.jafc.2c07781
J. Agric. Food Chem. 2023, 71, 660−670

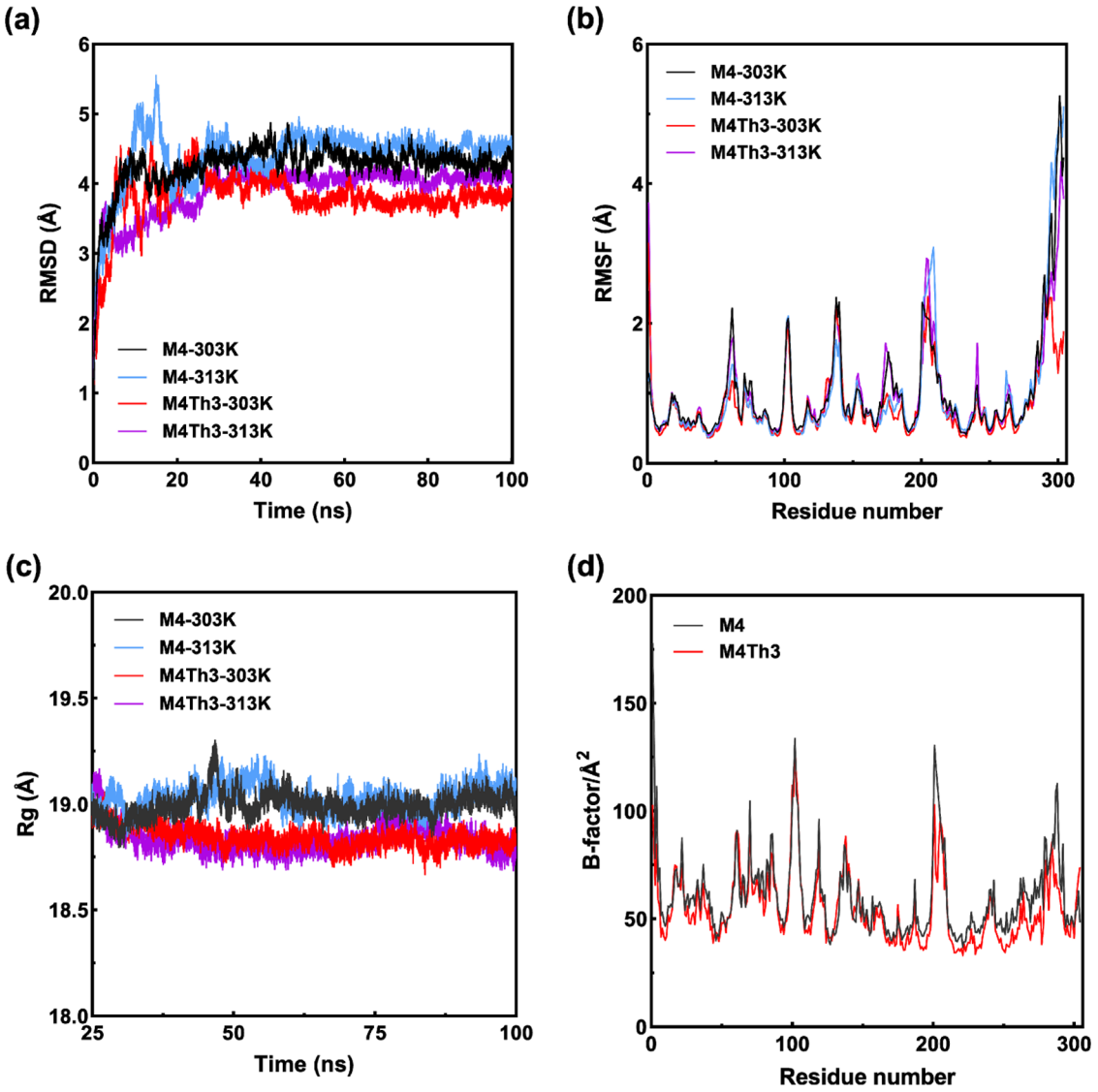

Figure 4. MD simulation analyses of M4 and M4Th3 at 303 and 313 K: (a) RMSD, (b) RMSF, (c) Rg values, and (d) B-factors.

S202, L203, S204, G205, and E208 were selected as hotspots for site-directed mutagenesis.

Loop 137−145 adjacent to sites 200−208 is composed of P137, E138, R139, S140, H141, Q142, H143, L144, and E145. As this longer loop is also located at the entrance of the active pocket, it is speculated that it could be related to the activity and thermostability. By aligning loop 137−145 among ancestral and descendent sequences, it was found that most of the residues were conservative. Among all of the residues, E138 is not conserved, displaying a more diverse distribution than the others. Hence, site 138 was also selected for site-directed mutagenesis.

Sites 276−284 (D276, R277, C278, R279, Y280, Y281, K282, S283, and H284) were adjacent to the C-terminus of the subunit. *Ni*HyuC-M4 is a homodimeric protein, and the C-termini of the two subunits are closely overlapped. The C-terminus of each subunit is freely extended outside of the main scaffold, which may affect the structural stability and the interaction between the two subunits. The sequence of sites 276−284 was compared with the 299 ancestor sequences to analyze its evolutionary conservatism. R277, Y280, and H284 were found to be the least conservative. Mutagenesis of these three residues was attempted to evaluate their effect on the stability of M4.

3.2. Greedy-Oriented Evolution of Thermostability. Using mutant M4 as the template, site-directed mutagenesis was performed on the above 10 sites. These sites were concisely mutated into other amino acids observed in the analysis of evolutionary consensus. After experimental verification, a total of nine single mutants with improved thermostability ($t_{1/2}$ (40 °C) >125% of M4) were obtained, including E138W, E138S, S202P, S204D, S204N, R277L, R277Q, H284T, and H284N. Among the above 10 sites, two mutants (E208D and R277E) displayed both improved thermostability and enzymatic activity, with specific activity >113% of M4 and $t_{1/2}$ (40 °C) >122% of M4 (Table S6).

To further improve the thermostability of D-carbamoylase and attenuate the "trade-off" between activity and stability, single mutants exhibiting $t_{1/2}$ (40 °C) >125% of M4 and specific activity >40% of M4 were selected for combinatorial mutagenesis, including E138W, E138S, S202P, S204D, S204N, E208D, R277L, R277Q, H284T, and H284N. This is regarded as greedy-oriented iterative combinatorial mutagenesis, which could rapidly yield mutants with significantly improved

https://doi.org/10.1021/acs.jafc.2c07781
J. Agric. Food Chem. 2023, 71, 660−670

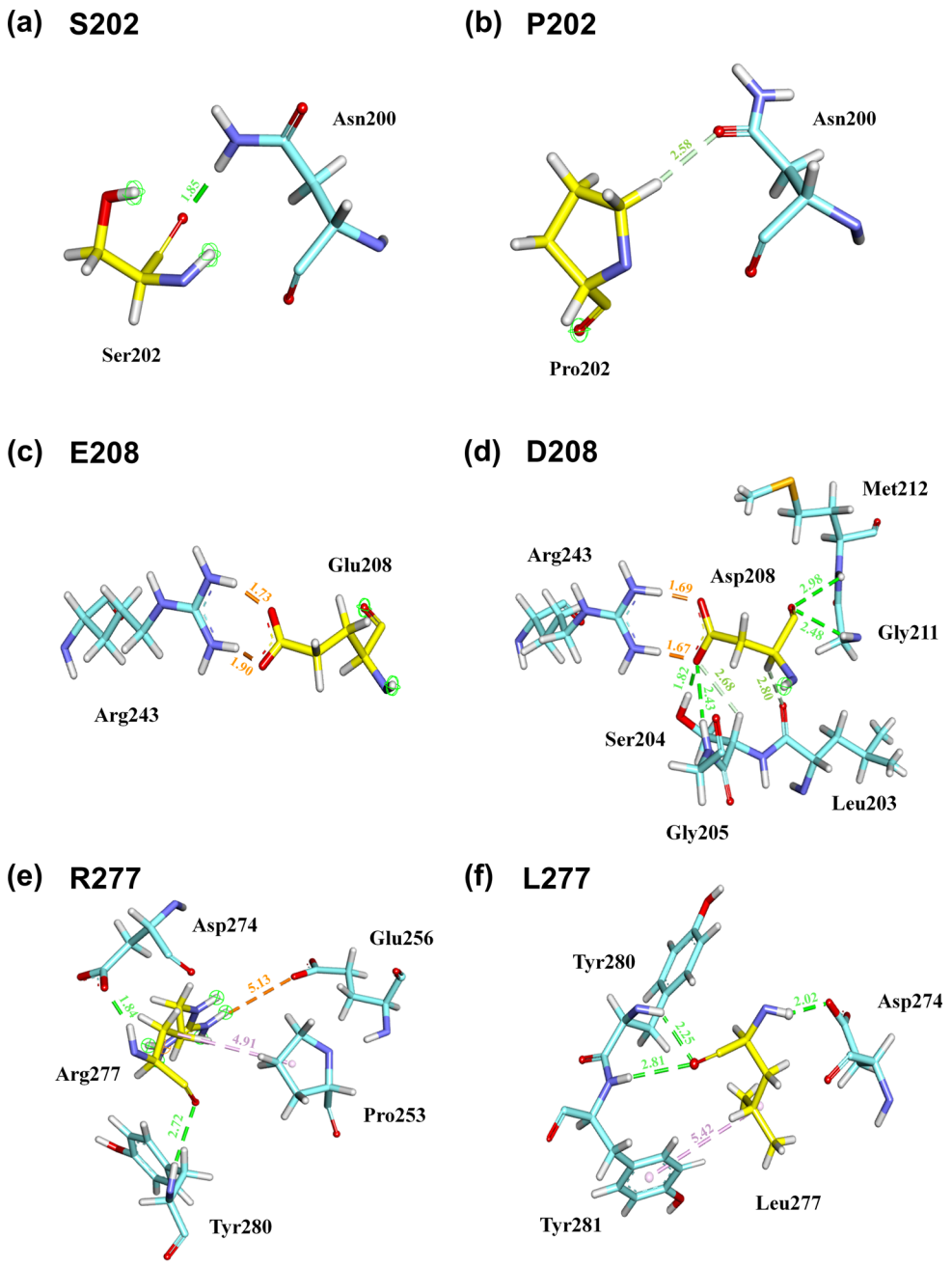

Figure 5. Interaction analyses of S202 (a), E208 (c), and R277 (e) with the surrounding residues in M4 and of P202 (b), D208 (d), and L277 (f) with the surrounding residues in M4Th3.

thermostability. Mutants with enhanced thermostability were selected as templates for the next round of combinatorial mutations.[43] Therefore, R277L (M4Th1) with significantly improved thermostability was selected as the starting template in the first round, despite its slightly decreased activity (Figure 1b). Other superior single mutants were introduced into mutant R277L, and the best double-mutant S202P/R277L (M4Th2) was obtained with a $t_{1/2}$ (40 °C) of 17.5 h. The $t_{1/2}$ (40 °C) values of E208D/R277L and S202P/E208D were 16.2 and 13.4 h, respectively, which were several times higher than that of their single mutants, demonstrating an obvious synergistic effect. When E208D was further introduced into M4Th2, a beneficial triple-mutant S202P/E208D/R277L (M4Th3) was achieved with significantly improved stability. The $t_{1/2}$ of M4Th3 at 40 °C increased from 1.3 to 36.5 h, which was 28.5 times that of M4 (Figure 2a). Most importantly, the catalytic efficiency (k_{cat}/K_m) of M4Th3 was 302 $min^{-1}·mM^{-1}$, comparable to 288 $min^{-1}·mM^{-1}$ of M4 (Table 1).

Furthermore, E138W, E138S, S204D, S204N, H284T, and H284N were introduced into M4Th3 to construct quadruple mutants. However, their thermostability decreased to different extents, in spite of similar specific activity. Then, the best quadruple mutant E138W/S202P/E208D/R277L (M4Th4) was also used as the template to incorporate S204D, S204N, H284T, and H284N (Figure 1b). Among all of the quintuple mutants, M4Th4−H284T (M4Th5) exhibited higher thermostability compared with M4Th4. However, the thermostability of M4Th5 was inferior to that of M4Th3 (Figure 1b). Based on the obvious negative epistatic effect of quadruple and

https://doi.org/10.1021/acs.jafc.2c07781
J. Agric. Food Chem. 2023, 71, 660−670

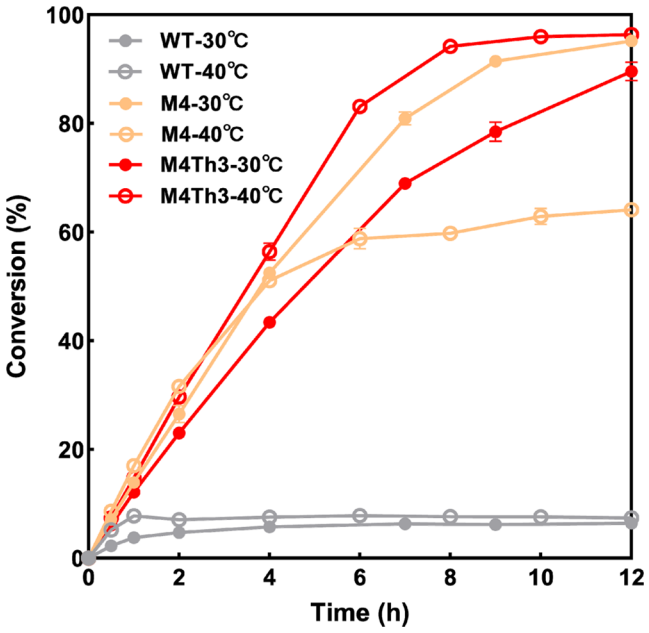

Figure 6. Reaction progress of *Ni*HyuC (WT), M4, and M4Th3 in the hydrolysis of 10 mM *N*−carbamoyl-D-tryptophan at 30 and 40 °C.

quintuple mutants, sextuple mutants were not constructed for further study. As a result, through greedy-oriented iterative combination mutagenesis, a triple mutant M4Th3 was obtained with significantly improved thermostability and desirable catalytic activity.

3.3. Characterization of Enzyme Properties. The effect of temperature on the activity of M4 and the above thermostable mutants was investigated. As shown in Figure 2b, the optimum temperature (T_{opt}) and specific activity of M4 were 45 °C and 3.49 U·mg^{-1}. The single mutant R277L displayed the highest activity of 2.65 U·mg^{-1} at 40 °C, which was lower than that of M4. However, it was found that the T_{opt} values of single mutants S202P and E208D were 50 °C, with specific activities of 3.40 and 4.71 U·mg^{-1} respectively. The best double mutant, S202P/R277L (M4Th2), had a T_{opt} of 40 °C and a specific activity of 2.51 U·mg^{-1}, indicating an antagonistic effect of S202P and R277L. However, it was noticed that the T_{opt} values of S202P/E208D and E208D/R277L were 50 and 40 °C, respectively. Moreover, the specific activity of S202P/E208D was 5.03 U·mg^{-1}, even higher than those of M4 and E208D. The best triple mutant S202P/E208D/R277L (M4Th3) exhibited a T_{opt} of 40 °C and a specific activity of 3.07 U·mg^{-1}. Apparently, L277 has a negative effect when combined with the other two mutations. For double and triple mutants harboring R277L, a decreased T_{opt} of 40 °C was observed, and the activity was also lower than that of M4. Both S202P and E208D are located at the entrance of the active pocket and have a synergistic/additive effect on the activity.

The Arrhenius equation reflects the relationship between the rate constant and the temperature. The activation energy for deactivation (E) calculated by the Arrhenius equation is used to compare the thermostability of proteins. The larger the difference in the activation energy for deactivation (ΔE, $\Delta E = E_{mutant} - E_{M4}$), the more stable the protein is. As shown in Table 2, the E value of the thermostable mutant M4Th3 is significantly higher than that of M4, with a ΔE as high as 200.4 kJ·mol^{-1}. Among single mutants, R277L exhibited the highest ΔE value of 111.2 kJ·mol^{-1}. Although the ΔE values of S202P and E208D were not high, a significantly increased ΔE and thermostability were observed for double mutants S202P/R277L and E208D/R277L when combined with R277L. Similarly, for S202P and E208D, the increase in T_{50}^{15} was only 1−2 °C, while the ΔT_{50}^{15} of R277L reached 2.2 °C. Although the thermostability of M4Th3 at 40 °C is significantly higher than that of M4, its T_m value is only 3.6 °C higher (Figure 2c). The increase in the T_m value of the mutant is not consistent with T_{50}^{15}, because T_{50}^{15} reflects the kinetic stability by detecting the change in enzyme activity with temperature, while T_m reflects the thermodynamic stability by detecting the change of the protein structure under a given temperature. Interestingly, it was found that the ΔE, T_{50}^{15}, and ΔT_m values of S202P, E208D, and R277L accumulated to be almost equivalent to the corresponding values of M4Th3, indicating additive or synergistic effect among these three single mutations.

In 2002, Oh and co-workers reported the engineering of a D-carbamoylase derived from *Agrobacterium tumefaciens* NRRL B11291 by DNA shuffling, and mutant 2S3 was obtained with improved antioxidative activity and thermostability. However, the catalytic efficiency was only 72% of WT.[44] In 2011, Zhang and co-workers attempted various strategies including epPCR, DNA shuffling, and iterative saturation mutagenesis to improve the thermostability of a highly soluble mutant DCase-M3 from *Ralstonia pickettii* CGMCC1596, and they finally obtained mutant D1 harboring 10 mutations with about 16 °C increase compared with the starting strain.[45] However, these methods involve complicated and intensive work in developing a saturation mutagenesis library and the screening of millions of mutant candidates. In contrast, using this ASR-guided evolutionary strategy, involving ancestral sequence reconstruction and evolutionary conservatism analysis, the thermostability of *Ni*HyuC was concisely and facilely engineered through a rational design. Compared with random mutagenesis and computation-guided virtual evolutionary strategies, this ASR-guided evolutionary strategy is time- and labor-saving and is especially suitable for evolving the thermostability due to the thermostable characteristics of ancestral enzymes. Mutants with significantly improved thermostability and comparable catalytic efficiency can be obtained more conveniently and rapidly using greedy-oriented iterative combinatorial mutagenesis, which may provide a promising approach for the engineering of thermostable D-carbamoylases.

3.4. Deconvolution Analysis. To further analyze the effect of single points (S202P, E208D, R277L) on M4Th3 and mechanisms underlying the decreased thermostability of M4Th4 and M4Th5, deconvolution analysis based on the obtained data of the $t_{1/2}$ values of single and double mutants ($t_{1/2}$ (40 °C) >100 min) was conducted, as illustrated in Figure 3. It can be found that when S202P, E208D, and R277L were combined to construct double mutants, doubled $t_{1/2}$ (40 °C) values were obtained. The result indicates an additive or synergistic effect among these three sites. The $t_{1/2}$ (40 °C) of R277L/H284N was significantly decreased, while the $t_{1/2}$ (40 °C) of another double mutant R277L/H284T was not determined due to its relatively low activity in preliminary screening. This result indicates that H284 has an obvious antagonistic effect on R277L. Although the $t_{1/2}$ (40 °C) of E138W/R277L is slightly higher than that of R277L, the combination did not significantly improve the stability. When site 138 was mutated from Glu to Trp or Ser, the recombinant proteins precipitated after elution, and only a low protein

https://doi.org/10.1021/acs.jafc.2c07781
J. Agric. Food Chem. 2023, 71, 660−670

concentration was obtained, which was not observed with other positions. Based on the above analysis, it is believed that E138 and H284 have antagonistic effects on R277L, which may explain the decreased thermostability of M4Th4 and M4Th5. Moreover, double mutants containing S204D or S204N were not determined due to their relatively low activities in the preliminary screening. Although S204D/N could improve the stability, its combination with other mutants resulted in a significant antagonistic effect. Site 204 is located at the entrance of the active pocket, and the mutation of Ser into Asp or Asn with a larger side chain could result in a decreased entrance tunnel, which is not favorable for the entry/exit of the substrate/product and therefore significantly decreased the activity.

3.5. MD Simulation and B-Factor Analysis. As shown in Figure 4, after 100 ns of MD simulations, the RMSD of M4 and M4Th3 stabilized within 0.5 Å. Both of them basically reached equilibrium after about 50 ns (Figure 4a). During 50−100 ns, the average RMSD of M4Th3 at 303 and 313 K was lower than that of M4, indicating that M4Th3 was more stable. Moreover, it was noted that with the increase in the temperature, the RMSD values of both M4Th3 and M4 increased, demonstrating that the overall structural stability decreased and the structure became looser. The RMSF results (Figure 4b) show that a mutation of these three sites (S202, E208, and R277) has no significant effect on the main scaffold of the protein, which is mainly manifested in a significantly decreased RMSF value of the C-terminus. Mutation R277L helps pull the free C-terminus closer to the main structure, which could improve the rigidity of the C-terminus structure, thereby promoting a more compact joint between two subunits. This also substantiates the feasibility of engineering the 276−284 region for a more restrained C-terminus structure, although it does not show a significantly increased hydrophobic force (as follows). For multi-subunit proteins, the subunit interface is crucial for stability, and the protein structure can be optimized by stabilizing the subunit interface. The Rg value of M4Th3 is about 0.25 Å lower than that of M4 (Figure 4c), which further proves that the mutant has a more compact overall protein structure and enhanced anti-unfolding ability after molecular modification.

It can be seen from Figure 4d that the B-factor of M4Th3 is significantly decreased after the mutation of sites S202, E208, and R277. Although the B-factor of the loop 200−207 is still high after mutation, it is understandable considering that the flexible loop is located at the entrance of the active pocket and affects the entry/exit of the substrate/product.

By intercepting the protein conformation in MD simulation, three sites 202, 208, and 277 on both M4 and M4Th3 were analyzed for intraprotein amino acid interactions. When S202 is mutated into P202, due to the unique pyrrole ring of Pro, the Cα−N single bond cannot rotate as freely as Ser, which reduces the flexibility of the protein backbone and improves the rigidity of the loop 200−207. Therefore, although only one hydrogen bond is formed with N200 at site 202 after mutation, the stability of M4 could be improved (Figure 5a,b).

With regard to E208 and surrounding amino acids, only two salt-bridge interactions were found between E208 and R243. As the crystal structure of M4 lacks S204 and G205, the interactions between E208 and the two sites cannot be analyzed (Figure 5c). D208 not only displays a salt-bridge interaction with R243 but also forms hydrogen bonds with L203, S204, G205, G211, and M212 (Figure 5d). The increased number of hydrogen bonds and the presence of D208 on the protein surface could help weaken the hydrophilicity of surface residues, increase hydrophobicity, and improve protein stability. The presence of S204 in the interactions network indicates that the single mutant S204D played a positive role in stability. However, the double mutant D204/D208 is repelled due to their identical negative charge, resulting in decreased stability. In previous studies, the single mutation R211G has been shown to significantly improve catalytic efficiency. In addition, mutation E208D introduces a smaller side chain and could enhance the interaction with G211, which is conducive to the entry/exit of the substrate/product, resulting in improved activity.[4]

In M4, R277 forms a π-alkyl hydrophobic interaction with the pyrrole ring on P253, a salt bridge with the oxygen on E256, and also a hydrogen bond with the oxygen atoms of D274 and Y281 (Figure 5e). When mutated to L277, it forms hydrogen bonds with oxygen atoms of D274 and Y280 and π-alkyl interaction with Y281 (Figure 5f). When the basic amino acid (Arg) was mutated into the nonpolar amino acid (Leu), the π-alkyl interaction with P253 and the salt bridge with E256 were lost. However, the emerged hydrogen-bonding interaction could increase the hydrophobicity and improve the stability. However, this does not seem to fully explain the contribution of R277L in improving the stability of M4. It should also be noted that residue 277 is adjacent to the subunit interface, and the C-terminus has a significantly decreased RMSF value after mutation (Figure 4b). The mutation of R277L might also stabilize the interface of the two subunits and thereby increase the structural stability.

3.6. Evaluating the Application of the Thermostable Mutant in the Synthesis of D-Tryptophan. Higher reaction temperatures can alleviate the requirements for a reaction cooling system, thereby reducing energy consumption. This can reduce both the cost and the environmental pollution caused by the cooling system. Moreover, the solubility and availability of insoluble substrates (such as hydantoin) can be improved by increasing the reaction temperature. The application potential of thermostable M4Th3 in the synthesis of D-tryptophan was evaluated and compared with that of the parental D-carbamoylases. At 30 °C, the conversion ratio of M4Th3 was slightly lower than that of M4 due to the lower activity of M4Th3, with final conversion ratios of 89.6 and 95.2%, respectively (Figure 6). However, at an elevated reaction temperature of 40 °C, the catalytic performance of M4 was significantly compromised due to its poor stability. In the beginning, M4Th3 exhibited slightly lower conversion than M4, and then, the conversion ratio increased steadily and reached as high as 96.4% at 12 h while that of M4 was only 64.1%. Moreover, WT D-carbamoylase (*Ni*HyuC) originally isolated from *N. indicus* had a final conversion of merely about 7% at both 30 and 40 °C. This could be ascribed to its low activity, high K_m value, and poor stability. This result further confirms that M4Th3 is more stable than M4.

In summary, the ancestral sequence reconstruction of a previously engineered beneficial mutant M4 of D-carbamoylase *Ni*HyuC was performed. Through ASR-based evolutionary conservatism analysis, hotspots were identified, and the thermostability of M4 was engineered by site-directed mutagenesis and greedy-oriented iterative combinatorial mutagenesis. Finally, thermostable M4Th3 was obtained with activity comparable to that of M4 and significantly increased thermostability. The $t_{1/2}$ at 40 °C of M4Th3 is 36.5 h, 28.5

https://doi.org/10.1021/acs.jafc.2c07781
J. Agric. Food Chem. 2023, 71, 660−670

times higher than that of M4. Structural and MD simulation analyses show that the improved thermostability of M4Th3 could arise from the intensified interactions within the protein, which render a more compact and stable conformation and also reduced the flexibility and increased the rigidity. Furthermore, the subunit interface is crucial for protein stability. R277L, located at the interface junction, could promote the binding between subunits by pulling the C-terminus closer to the main structure, thus promoting the structural stability of the protein. This study provides a concise approach for designing and engineering the thermostability of D-carbamoylase, which is a useful and industrially relevant biocatalyst for the synthesis of D-amino acids.

■ ASSOCIATED CONTENT

Supporting Information

The Supporting Information is available free of charge at https://pubs.acs.org/doi/10.1021/acs.jafc.2c07781.

Materials and methods; PCR reaction system (Table S1); PCR amplification procedure (Table S2); activation reaction system (Table S3); reaction process system (Table S4); primers for site-directed mutagenesis (Table S5); specific activity and thermostability of mutants (Table S6); activation energy for deactivation of mutants (Table S7); ancestral sequences reconstructed based on *Ni*HyuC-M4 (Figure S1); plot of SDS-PAGE analysis of nodes 151, 180, and 292 (Figure S2); nonconservative areas after sequence comparison among M4 and nodes 151, 180, 292: 137−145, 200−208, 276−284 (Figure S3); HPLC retention times of the substrate *N*-carbamoyl-D-tryptophan and the product D-tryptophan (Figure S4); the Ramachandran plot evaluation of the M4Th3 model (Figure S5); thermostability of the remaining single-point mutations at 40 °C (Figure S6); activation energy for deactivation of mutants (Figure S7); and T_m values of M4 and its mutants (Figure S8) (PDF)

■ AUTHOR INFORMATION

Corresponding Authors

Ye Ni − *Key laboratory of industrial Biotechnology, Ministry of Education, School of Biotechnology, Jiangnan University, Wuxi 214122 Jiangsu, China;* orcid.org/0000-0003-4887-7517; Email: yni@jiangnan.edu.cn

Guochao Xu − *Key laboratory of industrial Biotechnology, Ministry of Education, School of Biotechnology, Jiangnan University, Wuxi 214122 Jiangsu, China;* Email: guochaoxu@jiangnan.edu.cn

Authors

Jiamin Hu − *Key laboratory of industrial Biotechnology, Ministry of Education, School of Biotechnology, Jiangnan University, Wuxi 214122 Jiangsu, China*

Xiaoyu Chen − *Key laboratory of industrial Biotechnology, Ministry of Education, School of Biotechnology, Jiangnan University, Wuxi 214122 Jiangsu, China*

Lu Zhang − *Key laboratory of industrial Biotechnology, Ministry of Education, School of Biotechnology, Jiangnan University, Wuxi 214122 Jiangsu, China*

Jieyu Zhou − *Key laboratory of industrial Biotechnology, Ministry of Education, School of Biotechnology, Jiangnan University, Wuxi 214122 Jiangsu, China*

Complete contact information is available at: https://pubs.acs.org/10.1021/acs.jafc.2c07781

Author Contributions

J.H.: investigation, data curation, writing—original draft, validation. X.C.: formal analysis. L.Z.: formal analysis. J.Z.: conceptualization. G.X.: methodology, conceptualization, writing—review and editing, supervision, and funding acquisition. Y.N.: conceptualization, supervision, funding acquisition, writing—review and editing. All authors read and approved the submitted manuscript.

Notes

The authors declare no competing financial interest.

All data generated or analyzed during this study are included in this published article and its supporting information files.

Ethical statement This article does not contain any studies with human participants or animals performed by any of the authors.

■ ACKNOWLEDGMENTS

The authors are grateful to the National Key Research and Development Program (2018YFA0901700), the National Natural Science Foundation of China (22077054), the National first-class discipline program of Light Industry Technology and Engineering (LITE2018-07), and the Program of Introducing Talents of Discipline to Universities (111-2-06) for the financial support of this research. The authors are thankful for the support from the high-performance computing cluster platform of the School of Biotechnology, Jiangnan University.

■ REFERENCES

(1) Gao, X.; Ma, Q.; Zhu, H. Distribution, industrial applications, and enzymatic synthesis of D-amino acids. *Appl. Microbiol. Biotechnol.* **2015**, *99*, 3341−3349.

(2) Watabe, K.; Ishikawa, T.; Mukohara, Y.; Nakamura, H. Purification and characterization of the hydantoin racemase of *Pseudomonas sp.* strain NS671 expressed in *Escherichia coli*. *J. Bacteriol.* **1992**, *174*, 7989−7995.

(3) Nozaki, H.; Takenaka, Y.; Kira, I.; Watanabe, K.; Yokozeki, K. D-Amino acid production by *E. coli* co-expressed three genes encoding hydantoin racemase, D-hydantoinase and *N*-carbamoyl-D-amino acid amidohydrolase. *J. Mol. Catal. B: Enzym.* **2005**, *32*, 213−218.

(4) Liu, Y.; Xu, G.; Zhou, J.; Ni, J.; Zhang, L.; Hou, X.; Yin, D.; Rao, Y.; Zhao, Y.; Ni, Y. Structure-Guided Engineering of D-Carbamoylase Reveals a Key Loop at Substrate Entrance Tunnel. *ACS Catal.* **2020**, *10*, 12393−12402.

(5) Sapuntsova, S. G.; Mel'Nikova, N. P.; Deigin, V. I.; Kozulin, E. A.; Timoshin, S. S. Proliferative processes in the epidermis of patients with atopic dermatitis treated with thymodepressin. *Bull. Exp. Biol. Med.* **2002**, *133*, 488−490.

(6) Waring, M. J. Synthetic aspects of biologically active cyclic peptides—gramicidin S and tyrocidines. *Cell* **1980**, *21*, 591−592.

(7) Giuliano, F.; Varanese, L. Tadalafil: a novel treatment for erectile dysfunction. *Eur. Heart J. Suppl.* **2002**, *4*, H24−H31.

(8) Elafify, M.; Sadoma, N. M.; El Aal, S. F. A. A.; Bayoumi, M. A.; Ismail, T. A. Occurrence and D-Tryptophan Application for Controlling the Growth of Multidrug-Resistant Non-O157 Shiga Toxin-Producing *Escherichia coli* in Dairy Products. *Animals* **2022**, *12*, No. 922.

(9) Mukohara, Y.; Ishikawa, T.; Watabe, K.; Nakamura, H. A thermostable hydantoinase of *Bacillus stearothermophilus* NS1122A: cloning, sequencing, and high expression of the enzyme gene, and some properties of the expressed enzyme. *Biosci., Biotechnol., Biochem.* **1994**, *58*, 1621−1626.

(10) Martínez-Rodríguez, S.; Martinez-Gomez, A. I.; Rodriguez-Vico, F.; Clemente-Jimenez, J. M.; Heras-Vazquez, F. J. L. Carbamoylases: characteristics and applications in biotechnological processes. *Appl. Microbiol. Biotechnol.* **2010**, *85*, 441−458.
(11) Ikenaka, Y.; Nanba, H.; Yajima, K.; Yamada, Y.; Takano, M.; Takahashi, S. Thermostability reinforcement through a combination of thermostability-related mutations of *N*-carbamoyl-D-amino acid amidohydrolase. *Biosci., Biotechnol., Biochem.* **1999**, *63*, 91−95.
(12) Slomka, C.; Spath, G. P.; Lemke, P.; Skoupi, M.; Niemeyer, C. M.; Syldatk, C.; Rudat, J. Toward a cell-free hydantoinase process: screening for expression optimization and one-step purification as well as immobilization of hydantoinase and carbamoylase. *AMB Express* **2017**, *7*, No. 122.
(13) Andrade, J. M.; Peres, R. C. D.; Oesreicher, E. G.; Antunes, O. A. C.; Dariva, C. Immobilization of D-hydantoinase in polyaniline. *J. Mol. Catal. B: Enzym.* **2008**, *55*, 185−188.
(14) Pozo-Dengra, J.; Martínez-Gómez, A. I.; Martínez-Rodríguez, S.; Clemente-Jiménez, J. M.; Rodríguez-Vico, F.; Heras-Vázquez, F. J. L. Racemization study on different *N*-acetylamino acids by a recombinant *N*-succinylamino acid racemase from *Geobacillus kaustophilus* CECT4264. *Process Biochem.* **2009**, *44*, 835−841.
(15) Liu, Y.; Xu, G.; Han, R.; Dong, J.; Ni, Y. Identification of D-carbamoylase for biocatalytic cascade synthesis of D-tryptophan featuring high enantioselectivity. *Bioresour. Technol.* **2018**, *249*, 720−728.
(16) Wu, H.; Chen, Q.; Zhang, W.; Mu, W. Overview of strategies for developing high thermostability industrial enzymes: Discovery, mechanism, modification and challenges. *Crit. Rev. Food Sci. Nutr.* **2021**, 1−18.
(17) Kozome, D.; Uechi, K.; Taira, T.; Fukada, H.; Kubota, T.; Ishikawa, K.; Atomi, H. Structural Analysis and Construction of a Thermostable Antifungal Chitinase. *Appl. Environ. Microbiol.* **2022**, *88*, No. e0065222.
(18) Watanabe, K.; Ohkuri, T.; Yokobori, S.; Yamagishi, A. Designing thermostable proteins: Ancestral mutants of 3-isopropylmalate dehydrogenase designed by using a phylogenetic tree. *J. Mol. Biol.* **2006**, *355*, 664−674.
(19) Heinzelman, P.; Snow, C. D.; Wu, I.; Nguyen, C.; Villalobos, A.; Govindarajan, S.; Minshull, J.; Arnold, F. H. A family of thermostable fungal cellulases created by structure-guided recombination. *Proc. Natl. Acad. Sci. U.S.A.* **2009**, *106*, 5610−5615.
(20) Khersonsky, O.; Kiss, G.; Roethlisbergei, D.; Dym, O.; Albeck, S.; Houk, K. N.; Baker, D.; Tawfik, D. S. Bridging the gaps in design methodologies by evolutionary optimization of the stability and proficiency of designed Kemp eliminase KE59. *Proc. Natl. Acad. Sci. U.S.A.* **2012**, *109*, 10358−10363.
(21) Chen, J. J.; Chen, D.; Chen, Q. M.; Xu, W.; Zhang, W. L.; Mu, W. M. Computer-Aided Targeted Mutagenesis of *Thermoclostridium caenicola*D-Allulose 3-Epimerase for Improved Thermostability. *J. Agric. Food Chem.* **2022**, *70*, 1943−1951.
(22) Doble, M. V.; Obrecht, L.; Joosten, H.-J.; Lee, M.; Rozeboom, H. J.; Branigan, E.; Naismith, J. H.; Janssen, D. B.; Jarvis, A. G.; Kamer, P. C. J. Engineering Thermostability in Artificial Metalloenzymes to Increase Catalytic Activity. *ACS Catal.* **2021**, *11*, 3620−3627.
(23) Gumulya, Y.; Baek, J. M.; Wun, S. J.; Thomson, R. E. S.; Harris, K. L.; Hunter, D. J. B.; Behrendorff, J. B. Y. H.; Kulig, J.; Zheng, S.; Wu, X. M.; et al. Engineering highly functional thermostable proteins using ancestral sequence reconstruction. *Nat. Catal.* **2018**, *1*, 878−888.
(24) Bosch, S.; Sanchez-Freire, E.; del Pozo, M. L.; Cesnik, M.; Quesada, J.; Mate, D. M.; Hernandez, K.; Qi, Y. Y.; Clapes, P.; Vasic-Racki, D.; et al. Thermostability Engineering of a Class II Pyruvate Aldolase from *Escherichia coli* by in Vivo Folding Interference. *ACS Sustainable Chem. Eng.* **2021**, *9*, 5430−5436.
(25) Mateljak, I.; Alcalde, M. Engineering a Highly Thermostable High-Redox Potential Laccase. *ACS Sustainable Chem. Eng.* **2021**, *9*, 9632−9637.
(26) Guo, J.; Wang, Y.; Zhang, X.; Gao, W. J.; Cai, Z. Q.; Hong, T. T.; Man, Z. W.; Qing, Q. Improvement of the Catalytic Activity of Chitosanase BsCsn46A from *Bacillus subtilis* by Site-Saturation Mutagenesis of Proline121. *J. Agric. Food Chem.* **2021**, *69*, 11835−11846.
(27) Xu, Z.; Cen, Y. K.; Zou, S. P.; Xue, Y. P.; Zheng, Y. G. Recent advances in the improvement of enzyme thermostability by structure modification. *Crit. Rev. Biotechnol.* **2020**, *40*, 83−98.
(28) King, D. T.; Serrano-Negron, J. E.; Zhu, Y. P.; Moore, C. L.; Shoulders, M. D.; Foster, L. J.; Vocadlo, D. J. Thermal Proteome Profiling Reveals the O-GlcNAc-Dependent Meltome. *J. Am. Chem. Soc.* **2022**, *144*, 3833−3842.
(29) Deng, J. H.; Cui, Q. Electronic Polarization Is Essential for the Stabilization and Dynamics of Buried Ion Pairs in Staphylococcal Nuclease Mutants. *J. Am. Chem. Soc.* **2022**, *144*, 4594−4610.
(30) Kumar, S.; Sun, L.; Muralidhara, B. K.; Halpert, J. R.; Halpert, J. R. Engineering mammalian cytochrome P4502B1 by directed evolution for enhanced catalytic tolerance to temperature and dimethyl sulfoxide. *Protein Eng., Des. Sel.* **2006**, *19*, 547−554.
(31) Yu, Z.; Yu, H.; Xu, J.; Wang, Z.; Wang, Z.; Kang, T.; Chen, K.; Pu, Z.; Wu, J.; Yang, L.; Xu, G. Enhancing thermostability of lipase from *Pseudomonas alcaligenes* for producing L-menthol by the CREATE strategy. *Catal. Sci. Technol.* **2022**, *12*, 2531−2541.
(32) Risso, V. A.; Manssour-Triedo, F.; Delgado-Delgado, A.; Arco, R.; Barroso-delJesus, A.; Ingles-Prieto, A.; Godoy-Ruiz, R.; Gavira, J. A.; Gaucher, E. A.; Ibarra-Molero, B.; Sanchez-Ruiz, J. M. Mutational Studies on Resurrected Ancestral Proteins Reveal Conservation of Site-Specific Amino Acid Preferences throughout Evolutionary History. *Mol. Biol. Evol.* **2015**, *32*, 440−455.
(33) Schriever, K.; Saenz-Mendez, P.; Rudraraju, R. S.; Hendrikse, N. M.; Hudson, E. P.; Biundo, A.; Schnell, R.; Syren, P. O. Engineering of Ancestors as a Tool to Elucidate Structure, Mechanism, and Specificity of Extant Terpene Cyclase. *J. Am. Chem. Soc.* **2021**, *143*, 3794−3807.
(34) Trudeau, D. L.; Kaltenbach, M.; Tawfik, D. S. On the Potential Origins of the High Stability of Reconstructed Ancestral Proteins. *Mol. Biol. Evol.* **2016**, *33*, 2633−2641.
(35) Babkova, P.; Sebestova, E.; Brezovsky, J.; Chaloupkova, R.; Damborsky, J. Ancestral Haloalkane Dehalogenases Show Robustness and Unique Substrate Specificity. *ChemBioChem* **2017**, *18*, 1448−1456.
(36) Perez-Jimenez, R.; Ingles-Prieto, A.; Zhao, Z. M.; Sanchez-Romero, I.; Alegre-Cebollada, J.; Kosuri, P.; Garcia-Manyes, S.; Kappock, T. J.; Tanokura, M.; Holmgren, A.; et al. Single-molecule paleoenzymology probes the chemistry of resurrected enzymes. *Nat. Struct. Mol. Biol.* **2011**, *18*, 592−596.
(37) Gaucher, E. A.; Govindarajan, S.; Ganesh, O. K. Palaeotemperature trend for Precambrian life inferred from resurrected proteins. *Nature* **2008**, *451*, 704−702.
(38) Godoy-Ruiz, R.; Ariza, F.; Rodriguez-Larrea, D.; Perez-Jimenez, R.; Ibarra-Molero, B.; Sanchez-Ruiz, J. M. Natural selection for kinetic stability is a likely origin of correlations between mutational effects on protein energetics and frequencies of amino acid occurrences in sequence alignments. *J. Mol. Biol.* **2006**, *362*, 966−978.
(39) Gumulya, Y.; Huang, W. L.; D'Cunha, S. A.; Richards, K. E.; Thomson, R. E. S.; Hunter, D. J. B.; Baek, J. M.; Harris, K. L.; Boden, M.; De Voss, J. J.; et al. Engineering Thermostable CYP2D Enzymes for Biocatalysis Using Combinatorial Libraries of Ancestors for Directed Evolution (CLADE). *ChemCatChem* **2019**, *11*, 841−850.
(40) Patching, S. G. Efficient syntheses of 13C- and 14C-labelled 5-benzyl and 5-indolylmethyl L-hydantoins. *J. Labelled Compd. Radiopharm.* **2015**, *54*, 110−114.
(41) Musil, M.; Khan, R. T.; Beier, A.; Stourac, J.; Konegger, H.; Damborsky, J.; Bednar, D. FireProt(ASR): A Web Server for Fully Automated Ancestral Sequence Reconstruction. *Briefings Bioinf.* **2021**, *22*, No. bbaa337.
(42) Sumbalova, L.; Stourac, J.; Martinek, T.; Bednar, D.; Damborsky, J. HotSpot Wizard 3.0: web server for automated design

of mutations and smart libraries based on sequence input information. *Nucleic Acids Res.* **2018**, *46*, W356−W362.
(43) Cui, Y.; Chen, Y.; Liu, X.; Dong, S.; Tian, Ye.; Qiao, Y.; Mitra, R.; Han, J.; Li, C.; Han, X.; et al. Computational Redesign of a PETase for Plastic Biodegradation under Ambient Condition by the GRAPE Strategy. *ACS Catal.* **2021**, *11*, 1340−1350.
(44) Oh, K. H.; Nam, S. H.; Kim, H. S. Improvement of oxidative and thermostability of *N*-carbamoyl-D-amino acid amidohydrolase by directed evolution. *Protein Eng., Des. Sel.* **2002**, *15*, 689−695.
(45) Zhang, D. L.; Zhu, F. Y.; Fan, W. C.; Tao, R. S.; Yu, H.; Yang, Y. L.; Jiang, W. H.; Yang, S. Gradually accumulating beneficial mutations to improve the thermostability of *N*-carbamoyl-D-amino acid amidohydrolase by step-wise evolution. *Appl. Microbiol. Biotechnol.* **2011**, *90*, 1361−1371.

https://doi.org/10.1021/acs.jafc.2c07781
J. Agric. Food Chem. 2023, 71, 660−670